Structure, Vol. 9, 73–82, January, 2001, ©2001 Elsevier Science Ltd. All rights reserved. PII S0969-2126(00)00556-6

Molecular Basis for Regulatory Subunit Diversity in cAMP-Dependent Protein Kinase: Crystal Structure of the Type IIβ Regulatory Subunit

Thomas C. Diller,*† Madhusudan,† Nguyen-Huu Xuong,†‡ and Susan S. Taylor*†§

*Howard Hughes Medical Institute
University of California, San Diego
9500 Gilman Drive
La Jolla, California 92093

†Department of Chemistry and Biochemistry
University of California, San Diego
La Jolla, California 92093

‡Departments of Biology and Physics
University of California, San Diego
9500 Gilman Drive
La Jolla, California 92093

Summary

Background: Cyclic AMP binding domains possess common structural features yet are diversely coupled to different signaling modules. Each cAMP binding domain receives and transmits a cAMP signal; however, the signaling networks differ even within the same family of regulatory proteins as evidenced by the long-standing biochemical and physiological differences between type I and type II regulatory subunits of cAMP-dependent protein kinase.

Results: We report the first type II regulatory subunit crystal structure, which we determined to 2.45 Å resolution and refined to an R factor of 0.176 with a free R factor of 0.198. This new structure of the type IIβ regulatory subunit of cAMP-dependent protein kinase demonstrates that the relative orientations of the two tandem cAMP binding domains are very different in the type IIβ as compared to the type Iα regulatory subunit. Each structural unit for binding cAMP contains the highly conserved phosphate binding cassette that can be considered the "signature" motif of cAMP binding domains. This motif is coupled to nonconserved regions that link the cAMP signal to diverse structural and functional modules.

Conclusions: Both the diversity and similarity of cAMP binding sites are demonstrated by this new type II regulatory subunit structure. The structure represents an intramolecular paradigm for the cooperative triad that links two cAMP binding sites through a domain interface to the catalytic subunit of cAMP-dependent protein kinase. The domain interface surface is created by the binding of only one cAMP molecule and is enabled by amino acid sequence variability within the peptide chain that tethers the two domains together.

§To whom correspondence should be addressed (e-mail: staylor@ucsd.edu).

Introduction

The structural domain responsible for mediating biological effects of cyclic nucleotides as signaling molecules, specifically cAMP and cGMP, is conserved. In bacteria, this domain exists within the catabolite gene activator protein (CAP) [1]. In eukaryotes, it exists in proteins that regulate cAMP- and cGMP-dependent protein kinases (cAPK and cGPK) [2] and in other proteins that bind cyclic nucleotides (Figure 1) [3–5]. We now report a structure that enabled identification of a conserved binding cassette within the conserved core of cAMP binding domains (CBDs). This correlative structure demonstrates both the structural diversity of this domain even within a family of similar proteins and the diversity in the regulatory coupling of distinct cAMP binding domains to adjacent functional modules [6–8].

In the absence of cAMP, the two regulatory (R) and two catalytic (C) subunits of cAPK form a catalytically inactive, tetrameric holoenzyme complex. R subunits possess a conserved domain structure, which is comprised of a dimerization domain at the N terminus, two tandem cyclic-nucleotide binding domains at the C terminus, and a variable, interconnecting linker region (Figure 1). The linker region contains a substrate-like inhibitor sequence that docks to the active site cleft of the C subunit. Each R subunit cooperatively binds two cAMP molecules and releases concomitantly the C subunit as an active protein kinase [9]. R subunits associate with other macromolecules that restrict R subunit isoforms preferentially to distinct cellular locations [10]. R subunits, in addition to their regulatory function, protect C subunits from proteolysis [11], and this protective function can mitigate proteolytic inactivation of C subunits. Two general types of R subunits exist: type I (RI) and type II (RII). The RIIβ structure reported here represents the first type II R subunit structure. While all R subunits share the similar domain organization depicted in Figure 1, RI and RII differ in their molecular weights, isoelectric points, amino acid sequence, autophosphorylation capacities, and antigenicities. RI isoforms tend to be expressed in the cytoplasm of growing and transformed cells; RII isoforms predominate in the particulate fraction of differentiating and nontransformed cells [12–14]. RI and RII each have α and β subtypes with RIα and RIIα being expressed ubiquitously [15]. The β isoforms, expressed in a tissue-specific manner, are particularly prominent in brain [16]. RIIβ is the predominant isoform in adipose tissues [17].

Gene knockout experiments underscore unique properties of R subunit isoforms and identified significant physiological manifestations that are specifically attributable to the RIIβ isoform. For example, only knockout of the RIα isoform is lethal [17]. In RIIβ knockout mice, compensatory increases in RIα were observed [18, 19]. RIIβ knockout mice exhibit diminished white adipose

Key words: cAPK; regulatory subunit; RIIβ structure

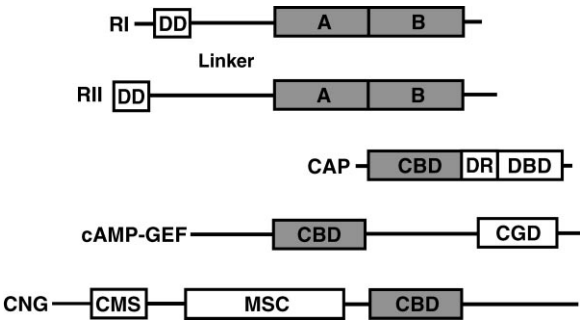

Figure 1. Modular Organization of Five Proteins That Contain Seven Homologous cAMP Binding Domains

RIα and RIIβ of cAPK contain N-terminal dimerization domains (DDs), variable linker regions, and tandem domains (A and B) that bind cAMP in a *syn* conformation [7]. CAP from *Escherichia coli* (*E. coli*) is comprised of an N-terminal cAMP binding domain (CBD) that binds cAMP in an *anti* conformation [8], a dimerization region (DR), and a C-terminal DNA binding domain (DBD). The cAMP-GEF protein has a CBD and guanine nucleotide exchange factor (GEF) domain (CGD) [5]. The cyclic-nucleotide-gated channel protein (CNG) has a putative calmodulin binding site (CMS), a membrane-spanning channel domain (MSC) and a CBD [45].

tissue (i.e., they display a lean phenotype) and deficits in complex motor behavior while displaying resistance to diet-induced obesity, haloperidol-induced gene expression, and catalepsy [17–22]. Further, RIIβ knockout mice exhibit decreased sensitivity to the sedative effects of ethanol consumption as measured by more rapid recovery from ethanol-induced sleep [23]. Despite increased voluntary consumption of ethanol, RIIβ knockout mice resist intoxicating effects: the acute effects of ethanol and voluntary ethanol consumption are linked to cAMP levels and cAPK activation [23]. RIIβ knockout mice display significantly decreased levels of C subunits, although RIIβ-deficient mice do not display decreased levels of either C subunits or cAPK activity [17–20]. These results demonstrate that R subunit isoforms are not functionally interchangeable, that isoform diversity is critical biologically, and that RIIβ may play an important role in diet-induced obesity [21]. These significant biological differences of R subunit isoforms must stem directly from unique differences at the level of molecular structure.

The crystal structure of the RIIβ deletion mutant reported here contributes substantially to understanding the paradox of diversity within a family of homologous proteins. Within the conserved structural core of each CBD, we identify key structural differences and a short, highly conserved amino acid sequence serving as the signature motif of CBDs: the phosphate binding cassette (PBC). Each cAMP binding site couples a conserved structural core through a nonconserved structural region to diverse signaling modules, thereby mediating domain interfaces and protein–protein interactions. Structural differences between RI and RII are sequence dependent, and differences in the relative position of the two tandem CBDs in each R subunit structure are not caused by a simple, flexible hinge or crystal packing. Rather, the two distinct structures are rigidly locked in place along the interface created by the surface-specific

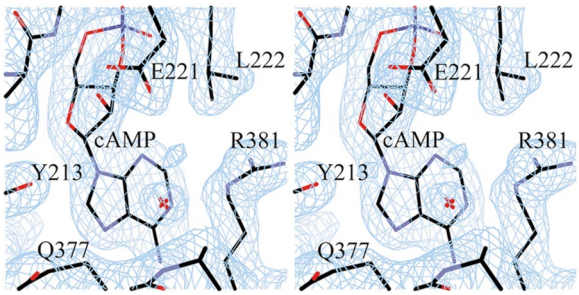

Figure 2. Stereoimage Showing the Electron Density of cAMP Bound within Site A of RIIβ

The depicted region represents a typical portion of the final sigma A–weighted $2F_o–F_c$ electron density map at 2.45 Å resolution with contouring at 2.0 σ using the program O [46].

binding of cAMP to site A. In addition to the sequence-specific governing of disparate domain orientations, highly conserved sequences within each subunit family, RI and RII, define unique signaling networks that link the cooperative binding of cAMP to the B domain, to the A domain, and then to the catalytic subunit binding site.

Results and Discussion

Structure Determination

The structure was solved based upon a model derived from a deletion mutant structure of cAPK RIα [7]. The deletion mutant of RIIβ contains two distinct CBDs (A and B), each consisting of a β barrel core. Based on the structural core of the RIα A domain, the program AMoRe [24] was used to determine successfully a phase solution only for domain A of RIIβ. The partially refined and modified phase solution for domain A of RIIβ led to a correct phase solution for domain B. Phase solutions were sought using either $P6_1$ or $P6_5$ as the space group for the RIIβ crystal [24]. The crystallographic R factor was significantly lower with a higher correlation coefficient for a phase solution in $P6_1$, and the solvent content of the crystal was calculated to be 70.8% with one molecule in the asymmetric unit [25]. Maximum likelihood refinement of the structural model using CNS [26] was performed, in conjunction with model building using sigma A–weighted electron density maps (Figure 2), to an R factor of 0.176 with a free R factor of 0.198 (Table 1).

The refined model consists of 274 amino acid residues, 2 cAMP molecules and 192 solvent atoms. Amino acid residues of the crystallized protein corresponding to the N terminus (112–129), a loop region (326–333), and the C terminus (413–416) are absent in the model owing to the lack of sufficiently well-defined electron density in sigma A–weighted $F_o–F_c$ and $2F_o–F_c$ maps. All modeled residues have properties less than 2.0 standard deviations from ideal values, and the overall stereochemical parameters of the model are classified by PROCHECK as being predominantly "BETTER" than typical X-ray structures solved at comparable resolution [27, 28].

Table 1. Data and Refinement Statistics [26, 38]

Space group	$P6_1$
Unit cell dimensions (Å)	
a = b =	161.62
c =	39.66
Resolution range (Å)	23.0–2.45
Unique reflections	21,958
Completeness (%)	
Overall (final shell)	98.6 (97.9)
Mosaicity	0.11
R_{merge}[a] (final shell)	0.052 (0.325)
R-factor$_r$[b] (R_{free}) [43]	0.176 (0.198)
RMS deviation from ideality	
bonds (Å)	0.006
angles (°)	1.3
Ramachandran angles (%) [27, 28, 44]	
most favored	93.0
additional allowed	7.0
B- factors (Å)[b]	
average	43.6
minimum	17.7
maximum	92.0

[a] $R_{merge} = \Sigma_{hkl}\Sigma_i|I - \langle I\rangle|/\Sigma_{hkl}\Sigma_i(I)$.
[b] R-factor$_r = \Sigma_{hkl}||F_{obs}| - \kappa|F_{calc}||/\Sigma_{hkl}|F_{obs}|$.

Cyclic AMP-Mediated Cooperativity

The structural features of the RIIβ deletion mutant include two jellyroll β barrels bounded and interconnected by conserved α helices (Figure 3). Each CBD is topologically similar and consists generally of eight β strands and four α helices (Figure 3). The β barrels serve as conserved cores for binding the phosphate of cAMP. Each β barrel is flanked by conserved α helices that link the β barrels to other functional modules. The surfaces presented by these α helices enable unique intramolecular and intermolecular interactions. Situated at the interface of the A and B domains, the A and B helices of the B domain (αA:B and αB:B) position side chains that interact with cAMP bound at site A (Figures 3 and 4). This region serves as an intramolecular lid to cover the open end of domain A's β barrel, thereby restricting cAMP within the A site. Kinetic data [9, 29, 30] and the numerous water molecules observed within this interfacial lid region of the crystal structure (Figure 4) provide evidence that this lid is easily (relative to the B domain) put in place or taken off. The solvated interface with its A-site cAMP enables dynamic transmission of conformational change from the A site through the B domain to the B site, and this transmission is critical for the cooperative binding and release of four cAMP molecules per RIIβ dimer upon holoenzyme formation [31].

Within the β barrel of the B domain, cAMP is buried in a much more hydrophobic environment relative to that of site A (Figure 4). The solvent accessibility of each cAMP, bound by RIIβ, coincides with kinetic measurements: the more highly solvated cAMP in the A site possesses faster on and off rates in comparison to the B-site cAMP [9, 29]. The lid that seals the B site of RIIβ is provided by domain B's long, C-terminal α-helix C (αB:C). This amphipathic helix is directly linked to the B domain's B helix (αB:B), which interacts directly with cAMP bound to site A. Any positional or conformational change of αB:B can be directly transmitted to αC:B at the B site and vice versa (Figure 3). The A-site cAMP, in contrast, is bound at the interface between the A and B domains, although predominantly within site A. Consequently, extensive interactions exist between residues of site A in the cAMP-bound state and the B domain (Figure 5). Sequestered within the basket of either cAMP binding site, cAMP is guarded from attack by phosphodiesterases typically present under physiological conditions.

In forming the holoenzyme complex, the C subunit binds the R subunit and effects a reversible conformational change that leads first to the release of the A-site cAMP (with a concomitant disruption of the R subunit's A:B domain interface) followed by the cooperative release of cAMP from the B site [9, 29, 31]. This series of distinct conformational states is reversed when the holoenzyme complex dissociates. During dissociation, cAMP can only be bound at site A after the B site is

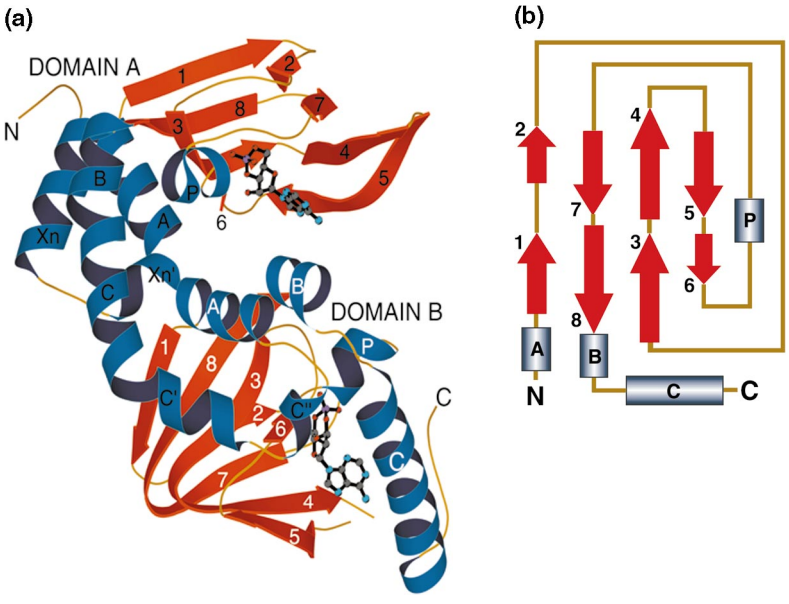

Figure 3. Overall Structure of RIIβ

(a) The MOLSCRIPT [47] depiction consists of two jellyroll β barrels with two cAMP molecules, one bound by each of the two domains. Residues were assigned to secondary structures using PROCHECK [27, 28], Insight II [40, 48], and CCP4 [49]. The α helices (blue ribbons) are identified by Roman letters; β strands (red ribbons) are labeled with a Greek numeral. Loop regions are brown. Labels for domain A are black, while domain B labels are white. The N terminus (N) begins with residue 130, and the C terminus (C) ends with residue 412. The break between β4 and β5 of domain B corresponds to residues (326–333).

(b) Topology of cAMP binding domains. The α helices are depicted as blue cylinders; β strands are represented by red arrows.

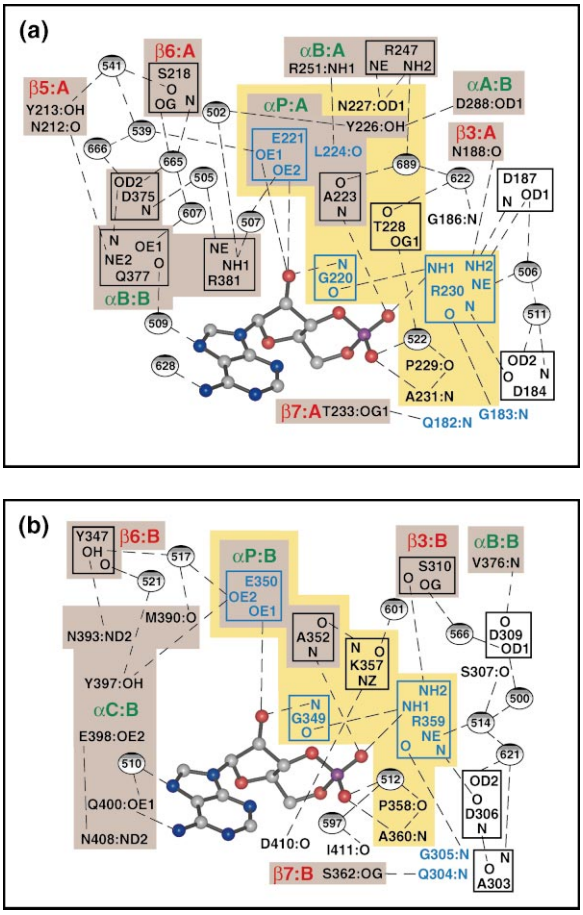

Figure 4. Hydrogen Bonds Surrounding cAMP

The network of conserved and nonconserved hydrogen bonds surrounding the two cAMP binding sites of RIIβ.

(a) Binding site A.

(b) Binding site B. Cyclic AMP molecules are rendered as balls and sticks with gray for carbon, blue for nitrogen, red for oxygen, and purple for the phosphorous atom. Hydrogen bonding is represented by dashed lines. Water oxygen atoms are illustrated as ovals with gradient shading and the uniquely identifying three-digit numeral assigned by the PDB file 1cx4. Tan-shaded boxes signify secondary structural elements identified in Figure 3; the labels for these boxes are either red for β strands or green for α helices. The regions encompassed by yellow lie within the conserved phosphate binding cassette. Amino acid residues with more than one hydrogen-bonding atom are boxed and labeled in either blue for invariant residues or black for nonconserved residues.

occupied [9, 30, 32]. Based on kinetic measurements, site A is only transiently vacant [9, 29, 31] and is not accessible to cAMP in the holoenzyme complex [32]; cAMP-free R subunits cannot be produced despite exhaustive dialysis. Consequently, site A acts as an intrinsic signaling switch that toggles between cAMP-bound, free R subunits and the cAMP-free, holoenzyme state. Transition between these states is affected by a complex, cooperative triad consisting of three sites: site A, site B, and a surface that interacts with the C subunit. The cAMP-bound state of RIIβ, as represented by the structure described here, demonstrates clearly (when compared to the previously solved RIα structure) that

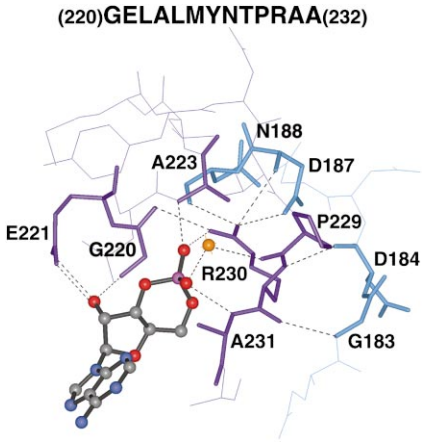

Figure 5. Phosphate Binding Cassette of RIIβ Domain A

Cyclic AMP is rendered as a ball-and-stick model [40]. The gold sphere represents a conserved solvent atom. Violet depicts the conserved PBC. Only the conserved shell of interactions is illustrated. Dashed lines represent hydrogen bonds conserved in available structures of CBDs.

the network of interactions orchestrated by site A (Figure 4) is isoform specific.

Phosphate Binding Cassette

Each cAMP binding site possesses conserved features while containing a distinct motif for interacting with its respective cAMP and peripheral modules. This is evidenced by each site's hydrogen-bonding pattern (Figure 4) elucidated from analyses of the refined structure. This network of hydrogen bonds may be altered substantially in the absence of cAMP. Imposed by the binding of a cyclic nucleotide, these networks of hydrogen bonds may not be sustained in the cyclic nucleotide's absence. Hydrogen-bonding interactions are conserved in the shell surrounding the phosphate end of each cAMP molecule. A highly conserved peptide segment, the phosphate binding cassette (PBC) (Figure 5) forms this shell and lies between β strands 6 and 7. The PBC is the most conserved feature (Figure 6) of these CBDs: it is the "signature" motif for cyclic-nucleotide binding domains.

Each basket-lining PBC contains two essential charged residues within a structurally conserved hydrophobic environment and a short phosphate binding (P) helix with conserved glutamic acid and leucine residues (Figures 5 and 6). In addition to containing the P helix, the PBC sequence begins with an invariant glycine, contains a conserved arginine and ends with an invariant alanine (Figure 6). Two charged amino acid side chains provide conserved contacts to the bound cyclic nucleotide (Figure 5). An arginine (230 and 359 in site A and B, respectively) lies at the bottom of each domain's basket-shaped β barrel. It bridges the phosphate of cAMP to β strand 3, two invariant glycines (220 and 349 at the N-terminal end of the PBC as well as 183 and 305) and two highly conserved aspartic acids (184 and 187 in site A, 306 and 309 in site B). A glycine (220 and 349) and glutamate (221 and 350) form hydrogen bonds with the ribose ring's 2′ hydroxyl. Within each PBC are five hydrophobic residues that are either invariant or very

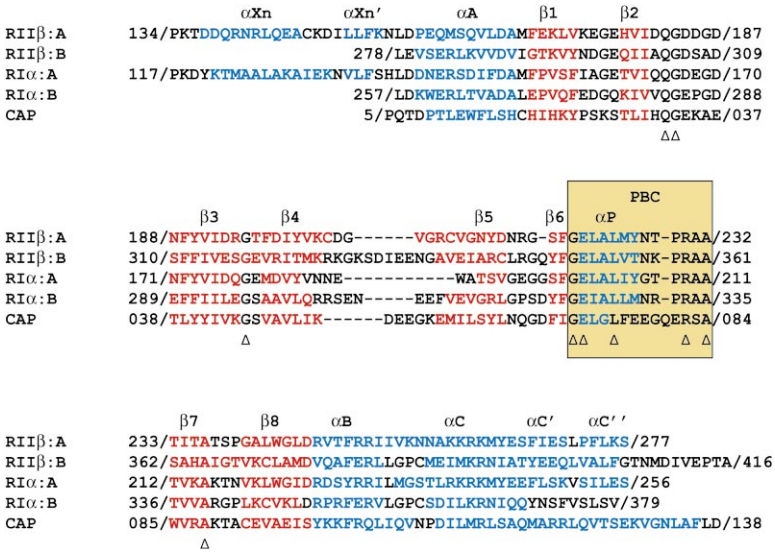

Figure 6. Sequence Alignment of Five cAMP Binding Domains

The aligned partial sequences of rat RIIβ (domains A and B), bovine RIα (domains A and B), and CAP from *E. coli* are depicted using the single-letter code for amino acids. Residue was derived from PDB files 2cgp (CAP), 1rgs (RIα), and 1cx4 (RIIβ). The conserved PBC is highlighted with a yellow-shaded box. Secondary structural elements are denoted above color-coded sequences: cyan denotes residues in α helices; red identifies residues in β strands. The symbol Δ identifies amino acid residues that are identical in all five of the aligned sequences, and dashes denote gaps for alignment.

highly conserved. Close structural inspection of nonconserved amino acids within the PBC indicate that hydrogen bonds to the main chain atoms of these residues are, in actuality, conserved in most cases (Figure 4). Of the five structures that have been solved, CAP has the only PBC with one additional residue that lies within a restrained, solvent-accessible loop of the PBC. This loop in CAP does not superimpose fully upon loops of R subunit PBCs (Figure 7).

Isoform Diversity of the Cooperative Triad

Within each CBD, the nonconserved, extended hydrogen-bond network enveloping the purine ring of cAMP (Figure 4) links each cAMP signal to other distinct functional modules. As shown in Figure 1, these modules include dimerization regions, DNA binding regions, other R-subunit structural units, and surfaces that interact with the C subunit of cAPK. Although the precise structural changes that accompany the cAMP-free state cannot be elucidated without determination of the holoenzyme structures of each R subunit isoform, analysis of the RIα and RIIβ structures in combination with available biochemical data enables identification of regions of RIIβ that likely interact with the C subunit. In RIα, the inhibitor site that docks to the active site cleft of the C subunit lies between residues 91 and 97 [33], and this region corresponds to residues 106 to 113 in RIIβ. These primary recognition sites for the C subunit are not visible in the crystal structures of either R subunit isoform. Additional, peripheral regions of the R subunit, defined by site-directed mutagenesis and analysis of deletion mutants, are protected from chemical modification in the holoenzyme complex and contribute to high affinity binding to the C subunit [34, 35]. These CBD A regions are highlighted in Figure 8 and include RIα residues 105–107, 140, 143, and 236–244 [34, 35]. Site A thus receives and transmits signals from both site B and the C subunit.

The relative orientation of the tandem CBDs is significantly different in the RIIβ structure as compared to the previously solved RIα structure, despite highly conserved amino acid sequences and structural elements. This is illustrated by the superimposition of either A or B domain core regions (Figure 8) and surface features (Figure 9). In the RIα crystallographic model, the distance between N7 of the A-site cAMP and O1P of the B-site cAMP is 29.5 Å. In contrast, this distance is only 19.3 Å in the RIIβ model. This difference underscores the unique interdomain conformational positions of RIIβ and RIα.

Closer examination of the structural differences between RIα and RIIβ domain orientations identifies a potential hinge point. Superimposition of the A domains from RIα and RIIβ (Figure 8) illustrates a region at the junction of αB:A and αC:A (e.g., residues 231–239 in RIα and residues 252–260 in RIIβ) that permits deviation in tertiary structure of the different R subunit types. This region represents a variable, predominantly α helical module that is neither amenable to structural superimposition of the different R subunit types nor technically part of the conserved core of either of the two CBDs (Figure 8). Comparative analysis of residue phi and psi angles in this region (Figure 7) indicates that these regions serve as a hinge for the variability in relative domain orientation, an orientation driven by sequence variability along the domain interface. The hinge-like difference in this region is stabilized by distinctly different side chain conformations of a conserved αXn′ phenylalanine (136 in RIα and 153 in RIIβ). Whether or not this region's hingelike quality is significant for the binding or release of cAMP might be more fully ascertained after determination of a holoenzyme structure.

The A-site cAMP, in contrast to the-site B cAMP, is bound at the interface between two domains, albeit predominantly within site A, and serves as a dowel pin that permits only one positional alignment of domain B relative to its respective domain A (Figure 9). This interdomain positioning cannot be attributed to a minute fraction of remotely situated, almost exclusively charged amino acid side chains at the protein's surface, although these side chains do enable Δ1–111 RIIβ molecules to form a static, ordered array within extremely fragile crys-

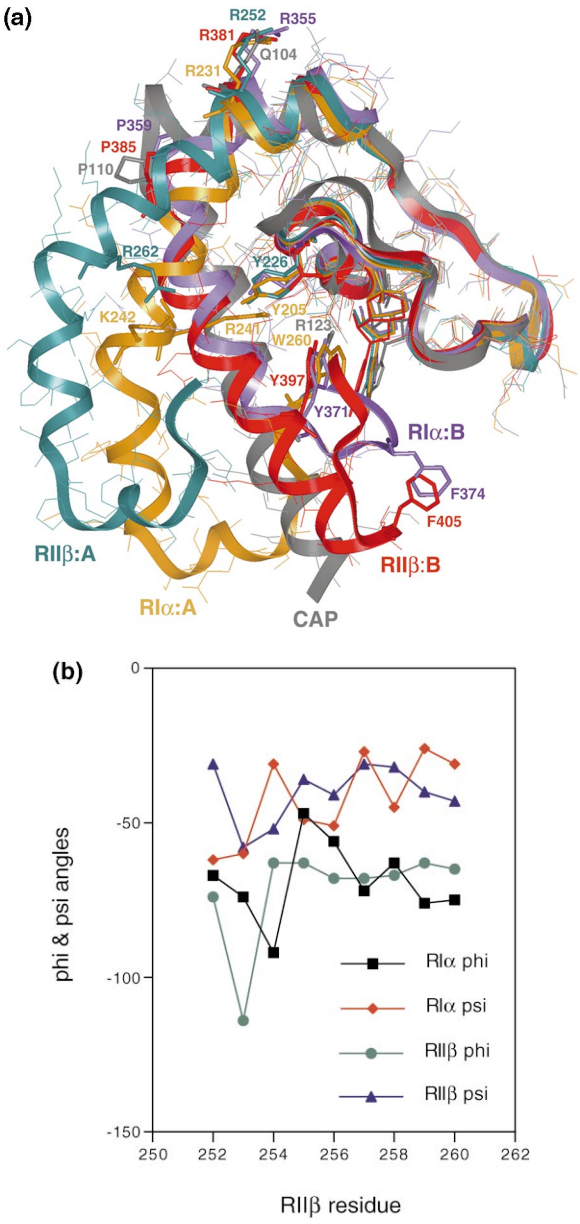

Figure 7. Comparison of CBDs

(a) Ribbon diagrams of five superimposed CBDs [40].

(b) Deviation of RIα and RIIβ structural superimposition: a plot of the phi and psi angles of residues belonging to hingelike regions at the C-terminal ends of A domain β barrels.

tals consisting of 70.8% solvent. Specifically, at the bottom of the cAMP acceptor pit of each A domain (Figure 9) lies the phosphate binding cassette's invariant arginine (Figures 5 and 6): 209 in RIα and 230 in RIIβ. Two other conserved surface features, immediately adjacent to the cAMP binding pit (Figure 9), enable specificity of both cAMP binding within site A and interdomain alignment. First, an invariant glutamic acid (200 in RIα and 221 in RIIβ) protrudes from domain A's PBC (Figure 9) to form conserved hydrogen bonds with cAMP (Figures 4 and 5). Second, a hydrophobic plateau formed by domain A residues accommodates the hydrophobic character of cAMP and is buried within the protein's sequestered core, surrounded by interdomain surface associations (Figure 9). This hydrophobic surface is comprised of residues in β strands β1:A (F156 in RIα and V173 in RIIβ), β3:A (F172, Y173, and I175 in RIα; F189, Y190, and I192 in RIIβ) and β6:A (F198 in RIα and F219 in RIIβ). Some variation in side chain type occurs (Figure 6), yet the topography of A domain interfacial surfaces remains very similar (Figure 9).

The interfacial surface of the B domain appears more diverse (Figure 9), yet it too provides only one specific location for binding cAMP within site A. At the central base of the binding surface within domain B is a conserved αB:B arginine (355 in RIα and 381 in RIIβ), although the interactions of this side chain differ between R subunit isoforms. Also illustrated in Figure 9 is a surface- and solvent-accessible "hole" in the B domain of RIα between R355 and W260. This feature is absent in RIIβ with its less solvent-accessible A-site cAMP (Figure 9). Surrounding this arginine are two conserved aspartic acid residues from opposite ends of domain B's amino acid sequence: N-terminal αA:B (267 in RIα and 288 in RIIβ) and C-terminal β8:B (349 in RIα and 375 in RIIβ). These aspartic acids are invariant within R subunits, not CAP (Figure 6). Side chains of two other prominent, nonconserved residues of domain B's interfacial surface that complete the lining of the cAMP bound within site A (Figures 4 and 9) belong either to αA:B (W260 in RIα and K285 in RIIβ) or αB:B (P351 in RIα and Q377 in RIIβ).

Overall, the interfacial electrostatic surface of the B domain presents a large proportion of charged side chains (Figure 9) as would be expected of a surface typically exposed to an aqueous environment. Conversely, the interfacial surface provided by domain A consists predominantly of neutral side chains (Figure 9) as would be expected of a more solvent inaccessible region. In the absence of cAMP, the interfacial surfaces of domains A and B do not appear to possess sufficiently complimentary regions to sustain interdomain association (Figure 9).

Further examination of residues that lie at the A:B domain interface or within the PBC illustrate additional important differences between RIα and RIIβ. Within the PBC of RIα's A domain, the conserved glutamic acid (200) is stabilized by hydrogen bonding to arginine 241 of αC:A, and this arginine in RIα is essential for the cooperative binding and release of cAMP to and from RIα cAMP binding sites A and B [36]. Arginine 241 in RIα corresponds to arginine 262 in RIIβ (Figure 6). Structurally, arginine 262 does not hydrogen bond to the conserved glutamic acid 221 in the PBC of RIIβ (Figure 4): the much greater distance between these two side chains (12.7 Å) stems from the positional shift of αC:A in RIIβ relative to the A domain's cAMP binding core in contrast to that observed in the RIα structure (Figure 7). Superimposition of the A domains of RIα and RIIβ demonstrates the positional difference of these arginine residues and αC:A (Figure 8), and this difference illustrates isoform-specific features of a highly cooperative signaling network. Additional mutational studies would be required to delineate the precise role of arginine 262 in RIIβ.

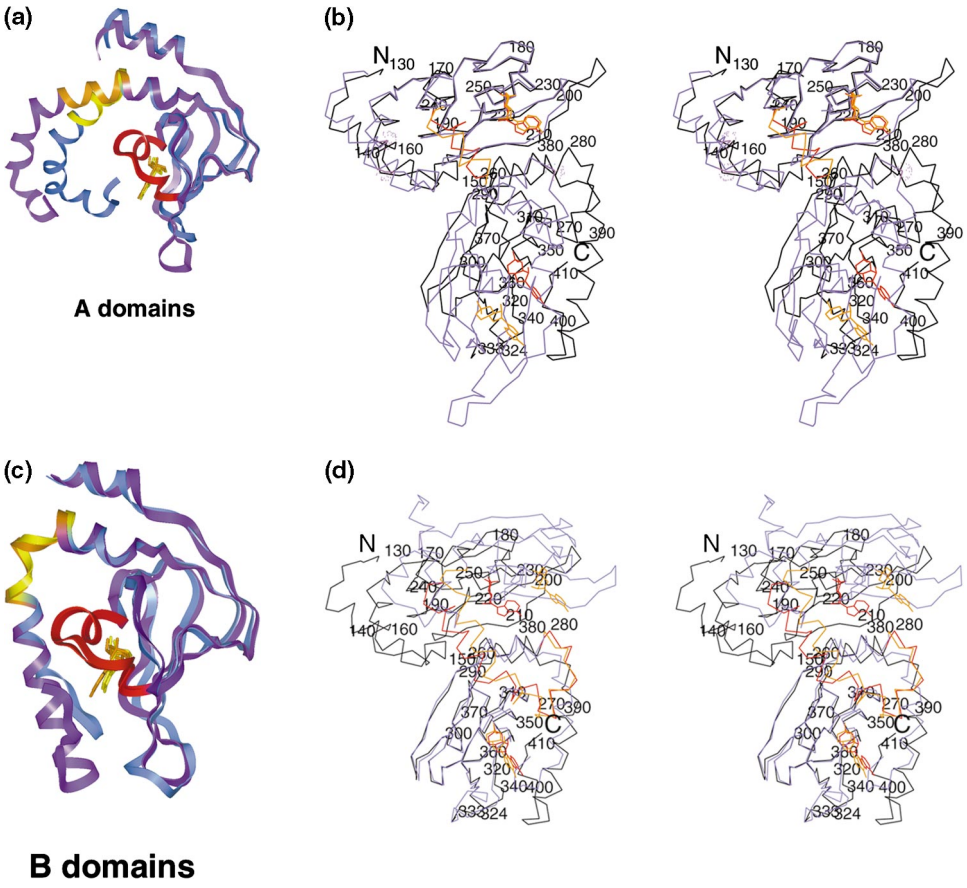

Figure 8. Structural Comparison of RIIβ and RIα Structures

(a, c) Superimposed ribbon diagrams of each cAMP binding domain (A domains and B domains) of RIα (cyan ribbons representing residues 139–376 except 231–239 and 355–363) and RIIβ (violet ribbons representing residues 156–412 except 252–260 and 381–389). Ribbons representing each domain's C-terminal hinge region are yellow for RIα residues 231–239 (domain A) and 355–363 (domain B) and orange for RIIβ residues 252–260 (domain A) and 381–389 (domain B). The conserved PBCs are all red, while cAMP molecules are rendered as sticks: yellow for RIα and orange for RIIβ.

(b) Stereoimage of superimposed A domains. Interdomain regions of structural deviation (i.e., within residues 231–239 of RIα and 252–260 of RIIβ) and bound cAMP molecules are colored yellow for RIα and orange for RIIβ with at least every tenth Cα atom of RIIβ labeled in black [40].

(d) Stereoimage of superimposed B domains. The Cα atoms of residues 232–259 of RIα are colored yellow, while residues 252–280 of RIIβ are colored orange with at least every tenth Cα atom of RIIβ labeled in black [40].

Biological Implications

Cyclic nucleotides like cAMP mediate signaling effects through cyclic-nucleotide binding domains, which have been conserved from bacteria to humans. The regulatory (R) subunits of cAMP-dependent protein kinase (cAPK) are the primary receptors for cAMP in mammalian cells, while the presence of two tandem cAMP binding domains (CBDs) is the hallmark of R subunits. The crystal structure of a deletion mutant of the RIIβ isoform described here, along with two previously solved structures containing CBDs, enabled identification of a signature motif, the phosphate binding cassette (PBC), for binding a cyclic nucleotide's phosphate.

R subunits are classified as either type I (RI) or type II (RII). Each of these two types is subdivided further into α and β isoforms, which are differentially localized in cells as well as being tissue specific. Gene knockout experiments highlight the biological importance of the isoforms and demonstrate uniquely important roles of RIIβ. Knockout of RIIβ, unlike knockout of RIα, is not lethal. Instead, RIIβ deficiency results in a lean phenotype, diminished white adipose tissue, and a decreased sensitivity to the sedative effects of ethanol consumption. Since these effects are uniquely attributable to lack of the RIIβ isoform, targeted disruption of RIIβ (through pharmaceutical intervention) can potentially abrogate diet-induced obesity and speed recovery from alcohol intoxication.

In designing specific inhibitors that preferentially target RIIβ without affecting vital functions of RIα, available structures of both these isoforms are invaluable. Structural comparison of RIα and RIIβ reveals altered dispositions of the B domain relative to the A domain in the two isoforms. The alteration in orientation stems from distinctly different domain interface surfaces and is allowed by a hingelike region between the cores of the tandem CBDs. The interface surfaces (Figure 9) are defined uniquely by amino acid sequence variability (Figure 6), a variability that also establishes unique networks of

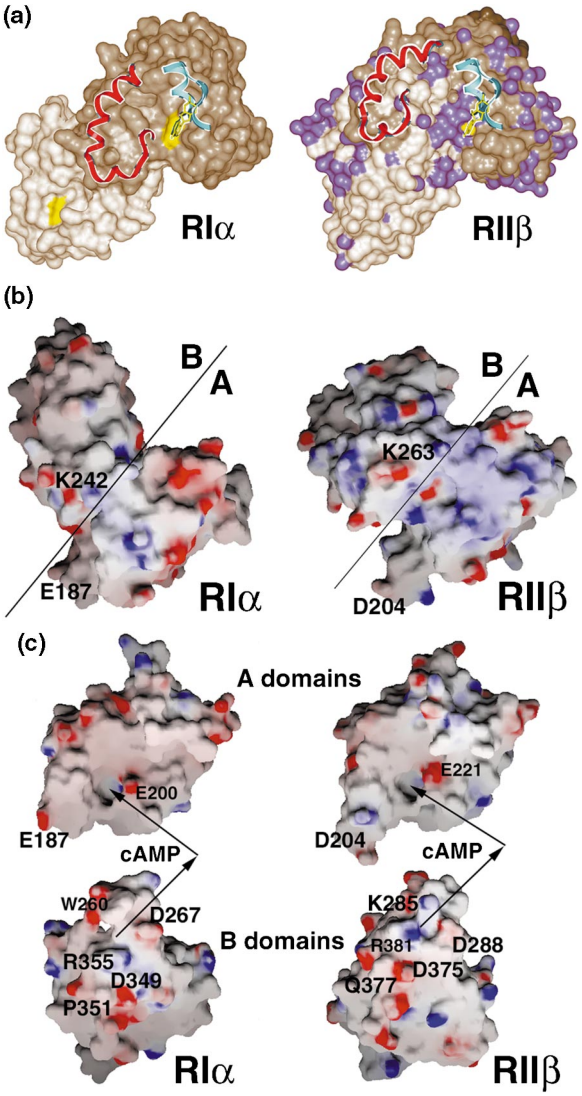

Figure 9. Surfaces of R Subunit Isoforms

Cyclic AMP binding cores of the A domains were superimposed prior to translation or rotation of surfaces.

(a) Cutaway Connolly surfaces [40] of RIα [7] and RIIβ. Cyclic AMP molecules are depicted by yellow sticks with their associated surfaces colored yellow. Main chain atoms of PBC residues are represented by turquoise ribbons. Red ribbons represent domain-interconnecting residues (236–260 in RIα or 256–280 in RIIβ), some of which have been shown to interact with regions of cAPK's C subunit. Surfaces of cAMP binding domain A are colored brown; domain B surfaces are colored tan. Surfaces for residues lying N terminal to domain A of RIIβ are colored gray; surfaces of water oxygen atoms (+) are colored violet.

(b) Top view of the domain-spanning α helices and interfacial regions of RIα and RIIβ. E187 and D204, included for perspective, belong to protruding, solvent-exposed loops between β4:A and β5:A. Black diagonal lines denote domain interfacial planes perpendicular to the plane of the paper. The surfaces of RIα (residues 115–376) and RIIβ (residues 130–325 and 334–412) were generated using GRASP [50].

(c) Side view of the domain interfaces of RIα and RIIβ in the absence of cAMP in site A. Following superimposition of the cAMP binding domain A cores of RIα and RIIβ, each surface was rotated to bring its respective interfacial A domain surface (A) into the plane of the paper facing outward. Each respective B domain surface (B) was then rotated 180° relative to its respective, rotated A domain surface. The positions of the aligning cAMP pins (cAMP) are denoted with arrows. Surface features are labeled for select residues.

interactions. These networks extend throughout each R subunit to mediate cooperative interactions between cAMP and the C subunit.

Experimental Procedures

Data Collection and Phase Solution

X-ray diffraction data were collected at the Stanford Synchrotron Radiation Laboratory (SSRL) on a single crystal [37]. Data were indexed and processed using DENZO and scaled with SCALEPACK [38]. Phases were generated by molecular replacement using a truncated model of one CBD of another cAPK regulatory subunit isoform (residues 113–237 of RIα with one bound cAMP molecule from PDB file 1rgs) [7]. Despite locating one domain of one molecule belonging to space group $P6_1$ with an initial R factor of 56.5%, locating additional domains, with or without cAMP, remained elusive. Based upon sequence comparison of rat RIIβ to bovine RIα, each variant residue was converted to an alanine in the starting model. This model was subjected to rigid body refinement using CNS [26]. Engh and Huber parameter and topology files used for cAMP were generated by modifying existing nucleic acid files [39]. AMoRe and the model of the single, partially refined domain was then used to determine a phase solution for one additional CBD in the asymmetric unit [24], although crystal packing analysis [40] indicated that the crystal's unit cell could accommodate four.

Initial correlation coefficients (10.1 and 14.5) were lower and initial R factors (55.4% and 54.0%) were higher than expected for the two-domain solution, and packing analysis indicated regions of potential overlap between symmetry-related molecules. Sigma A–weighted electron density maps were interpretable using TOM/FRODO [41], yet initial maps indicated a correct phase solution for only one of the two domains. When initial refinement did not reduce the R factor of the model, RIα residues 113–118, 180–200, and 236–237 were deleted from the search model. Molecular replacement procedures were then repeated. This led to the solution for two domains. Correlation coefficients were 15.6 and 17.2; initial R factors were 52.8% and 52.0%. Packing analysis [40] indicated a shift in orientation of the second domain relative to the first with no overlap between symmetry-related molecules.

Refinement

Maximum-likelihood refinement with sigma A weighting was performed with CNS protocols: rigid-body refinement, Powell minimization, simulated annealing from 2500°C, and individual B-factor refinement [26]. Sigma A–weighted maps produced using CNS [26] were reformatted using MAPMAN [42]. Side chains that subsequently became visible in electron density maps (sigma A weighted F_o–F_c and $2F_o$–F_c) enabled revision of the model. Refinement and model revision continued in an iterative fashion until nearly all alanine residues were converted to their proper amino acid. Stepwise revision of the crystallographic model progressed based on frequent PROCHECK analyses [27, 28] to a crystallographic R factor of 23%, at which point electron densities were assigned and verified as water molecules using CNS [26] and sigma A–weighted electron density maps [41, 42].

Acknowledgments

We specifically thank D. B. Huang, S. Dempsey, E. Radzio-Andzelm, A. Yap, K. Cowtan, L. F. Ten Eyck, P. Akamine, J. Canaves, and X. Cheng for assistance and helpful discussions. We acknowledge H. Parge for data collection at Agouron. We gratefully acknowledge C. D. Stout of The Scripps Research Institute (La Jolla, CA) and Agouron Pharmaceuticals (La Jolla, CA) for enabling us to collect data with their resources. We are also grateful to SSRL and its staff for assistance with synchrotron data collection. Work was supported by the National Institutes for Health (GM34921) to S. S. T. T. C. D. was also supported through the Lucille P. Markey Charitable Trust Fund and a National Science Foundation predoctoral fellowship.

Received: May 10, 2000
Revised: October 30, 2000
Accepted: November 10, 2000

References

1. Mitra, S., Zubay, G., and Landy, A. (1975). Evidence for the preferential binding of the catabolite gene activator protein (CAP) to DNA containing the lac promoter. Biochem. Biophys. Res. Commun. *67*, 857–863.
2. Shabb, J.B., and Corbin, J.D. (1992). Cyclic nucleotide-binding domains in proteins having diverse functions. J. Biol. Chem. *267*, 5723–5726.
3. Nakamura, T., and Gold, G.H. (1987). A cyclic nucleotide-gated conductance in olfactory receptor cilia. Nature *325*, 442–444.
4. Ludwig, J., Margalit, T., Eismann, E., Lancet, D., and Kaupp, U.B. (1990). Primary structure of cAMP-gated channel from bovine olfactory epithelium. FEBS Lett. *270*, 24–29.
5. Kawasaki, H., et al. (1998). A family of cAMP-binding proteins that directly activate Rap1. Science *282*, 275–279.
6. Weber, I.T., Steitz, T.A., Bubis, J., and Taylor, S.S. (1987). Predicted structures of cAMP binding domains of type I and type II regulatory subunits of cAMP-dependent protein kinase. Biochemistry *26*, 343–351.
7. Su, Y., et al. (1995). Regulatory subunit of protein kinase A: structure of deletion mutant with cAMP binding domains. Science *269*, 807–813.
8. Weber, I.T., and Steitz, T.A. (1987). Structure of a complex of catabolite gene activator protein and cyclic AMP refined at 2.5 Å resolution. J. Mol. Biol. *198*, 311–326.
9. Øgreid, D., and Døskeland, S.O. (1981). The kinetics of the interaction between cyclic AMP and the regulatory moiety of protein kinase II. FEBS Lett. *129*, 282–286.
10. Scott, J.D., and McCartney, S. (1994). Localization of A-kinase through anchoring proteins. Mol. Endo. *8*, 5–11.
11. Hemmings, B.A. (1986). cAMP mediated proteolysis of the catalytic subunit of cAMP-dependent protein kinase. FEBS Lett. *196*, 126–130.
12. Corbin, J.D., Keely, S.L., and Park, C.R. (1975). The distribution and dissociation of cyclic adenosine 3′:5′-monophosphate-dependent protein kinases in adipose, cardiac, and other tissues. J. Biol. Chem. *250*, 218–225.
13. De Camilli, P., Moretti, M., Donini, S.D., Walter, U., and Lohmann, S.M. (1986). Heterogenous distribution of the cAMP receptor protein RII in the nervous system: evidence for its intracellular accumulation on microtubules, microtubule-organizing centers, and in the area of the Golgi complex. J. Cell Biol. *103*, 189–203.
14. Rubin, C.S., Rangel-Aldao, R., Sarkar, D., Erlichman, J., and Fleischer, N. (1979). Characterization and comparison of membrane-associated and cytosolic cAMP-dependent protein kinases. J. Biol. Chem. *254*, 3797–3805.
15. Hofmann, F., Beavo, J.A., Bechtel, P.J., and Krebs, E.G. (1975). Comparison of adenosine 3′:5′-monophosphate-dependent protein kinases from rabbit skeletal and bovine heart muscle. J. Biol. Chem. *250*, 7795–7801.
16. Scott, J.D., et al. (1987). The molecular cloning of a type II regulatory subunit of the cAMP-dependent protein kinase from rat skeletal muscle and mouse brain. Proc. Natl. Acad. Sci. USA *84*, 5192–5196.
17. Cummings, D.E., et al. (1996). Genetically lean mice result from targeted disruption of the RIIβ subunit of protein kinase A. Nature *382*, 622–626.
18. Amieux, P.S., et al. (1997). Compensatory regulation of RIα protein levels in protein kinase A mutant mice. J. Biol. Chem. *272*, 3993–3998.
19. Brandon, E.P., Idzerda, R.L., and McKnight, G.S. (1997). PKA isoforms, neural pathways, and behaviour: making the connection. Curr. Opin. Neurobiol. *7*, 397–403.
20. Planas, J.V., Cummings, D.E., Idzerda, R.L., and McKnight, G.S. (1999). Mutation of the RIIβ subunit of protein kinase A differentially affects lipolysis but not gene induction in white adipose tissue. J. Biol. Chem. *274*, 36281–36287.
21. McKnight, G.S., et al. (1998). Cyclic AMP, PKA, and the physiological regulation of adiposity. Recent Prog. Horm. Res. *53*, 139–159.
22. Adams, M.R., Brandon, E.P., Chartoff, E.H., Idzerda, R.L., Dorsa, D.M., and McKnight, G.S. (1997). Loss of haloperidol induced gene expression and catalepsy in protein kinase A-deficient mice. Proc. Natl. Acad. Sci. USA *94*, 12157–12161.
23. Thiele, T.E., Willis, B., Stadler, J., Reynolds, J.G., Bernstein, I.L., and McKnight, G.S. (2000). High ethanol consumption and low sensitivity to ethanol-induced sedation in protein kinase A-mutant mice. J. Neurosci. *20*, 1–6.
24. Navaza, J. (1994). AMoRe: an automated package for molecular replacement. Acta Crystallogr. *A50*, 157–163.
25. Matthews, B.W. (1968). Solvent content of protein crystals. J. Mol. Biol. *33*, 491–497.
26. Brünger, A.T., et al. (1998). Crystallography and NMR system: a new software suite for macromolecular structure determination. Acta Crystallogr. *D54*, 905–921.
27. Laskowski, R.A., Moss, D.A., and Thornton, J.M. (1993). Main-chain bond lengths and bond angles in protein structures. J. Mol. Biol. *231*, 1049–1067.
28. Laskowski, R.A., MacArthur, M.W., Moss, D.A., and Thornton, J.M. (1993). PROCHECK—a program to check the stereochemical quality of protein structures. J. Appl. Cryst. *26*, 283–291.
29. Øgreid, D., and Døskeland, S.O. (1981). The kinetics of association of cyclic AMP to the two types of binding sites associated with protein kinase II from bovine myocardium. FEBS Lett. *129*, 287–292.
30. Rannels, S.R., and Corbin, J.D. (1981). Studies on the function of the two intrachain cAMP binding sites of protein kinase. J. Biol. Chem. *256*, 7871–7876.
31. Øgreid, D., and Døskeland, S.O. (1982). Activation of protein kinase isoenzymes under near physiological conditions: evidence that both types (A and B) of cAMP binding sites are involved in the activation of protein kinase by cAMP and 8-N_3-cAMP. FEBS Lett. *150*, 161–166.
32. Herberg, F.W., Taylor, S.S., and Dostmann, W.R.G. (1996). Active site mutations define the pathway for cooperative activation of cAMP-dependent protein kinase. Biochemistry *35*, 2934–2942.
33. Potter, R.L., and Taylor, S.S. (1979). Relationships between structural domains and function in the regulatory subunit of cAMP-dependent protein kinases I and II from porcine skeletal muscle. J. Biol. Chem. *254*, 2413–2418.
34. Gibson, R.M., Ji-Buechler, Y., and Taylor, S.S. (1997). Interaction of the regulatory and catalytic subunits of cAMP-dependent protein kinase: electrostatic sites on the type Iα regulatory subunit. J. Biol. Chem. *272*, 16343–16350.
35. Huang, L.J., and Taylor, S.S. (1998). Dissecting cAMP binding domain A in the RIα subunit of cAMP-dependent protein kinase: distinct subsites for recognition of cAMP and the catalytic subunit. J. Biol. Chem. *273*, 26739–26746.
36. Symcox, M.M., Cauthron, R.D., Øgreid, D., and Steinberg, R.A. (1994). Arg-242 [Arg-241] is necessary for allosteric coupling of cyclic AMP-binding sites A and B of RI subunit of cyclic AMP-dependent protein kinase. J. Biol. Chem. *269*, 23025–23031.
37. Diller, T.C., Xuong, N.-H., and Taylor, S.S. (2000). Type IIβ regulatory subunit of cAMP-dependent protein kinase: purification strategies to optimize crystallization. in press.
38. Otwinowski, Z., and Minor, W. (1997). Processing of x-ray diffraction data collected in oscillation mode. Methods Enzymol. *276*, 307–326.
39. Engh, R.A., and Huber, R. (1991). Accurate bond and angle parameters for x-ray protein-structure refinement. Acta Crystallogr. *A47*, 392–400.
40. Insight II. (1998). Version 98.0, Molecular Modeling System, Molecular Simulations Inc., San Diego, CA.
41. Cambillau, C., and Horjales, E. (1987). TOM: a FRODO subpackage for protein-ligand fitting with interactive energy minimization. J. Mol. Graph. *5*, 174–177.
42. Kleywegt, G.J., and Jones, T.A. (1996). xdlMAPMAN and xdlDATAMAN—programs for reformatting, analysis and manipulation of biomacromolecular electron-density maps and reflection data sets. Acta Crystallogr. *D52*, 826–828.

43. Brünger, A.T. (1992). The free R value: a novel statistical quantity for assessing the accuracy of crystal structures. Nature *355*, 472–474.
44. Ramachandran, G.N., and Sasisekharan, V. (1968). Conformation of polypeptides and proteins. Adv. Prot. Chem. *23*, 283–438.
45. Bönigk, W., et al. (1999). The native rat olfactory cyclic nucleotide-gated channel is composed of three distinct subunits. J. Neurosci. *19*, 5332–5347.
46. Jones, T.A., Zou, J.Y., Cowan, S.W., and Kjeldgaard, M. (1991). Improved methods for building protein models in electron density maps and the location of errors in these models. Acta Crystallogr. A *47*, 110–119.
47. Kraulis, P.J. (1991). MOLSCRIPT: a program to produce both detailed and schematic plots of protein structures. J. Appl. Cryst. *24*, 946–950.
48. Kabsch, W., and Sander, C. (1983). Dictionary of protein secondary structure: pattern recognition of hydrogen-bonded and geometrical features. Biopolymers *22*, 2577–2637.
49. CCP4 (Collaborative Computational Project 4). (1994). The CCP4 suite: programs for protein crystallography. Acta Crystallogr. D *50*, 760–763.
50. Nicholls, A., Sharp, K.A., and Honig, B. (1991). Protein folding and association: insights from the interfacial and thermodynamic properties of hydrocarbons. Proteins *11*, 281–296.

Accession Number

The Protein Data Bank accession code is 1cx4.

Note Added in Proof

The paper cited in this text as [37] has been published in Protein Expression and Purification, Vol. 20, pp. 357–364.